

Report Number 12/28

Non-linear effects on Turing patterns: time oscillations and chaos.

by

J.L. Aragon, R.A. Barrio, T.E. Woolley, R.E. Baker, P.K. Maini



Oxford Centre for Collaborative Applied Mathematics
Mathematical Institute
24 - 29 St Giles'
Oxford
OX1 3LB
England

Non-linear effects on Turing patterns: time oscillations and chaos.

J.L. Aragón¹, R.A. Barrio², T.E. Woolley³, R.E. Baker⁴, P.K. Maini^{4,5}

¹*Departamento de Nanotecnología, Centro de Física Aplicada y Tecnología Avanzada, Universidad Nacional Autónoma de México, Apartado Postal 1-1010, Querétaro 76000, México.*

²*Departamento de Física Química, Instituto de Física, Universidad Nacional Autónoma de México, Apartado Postal 01000, 76230 D.F., México.*

³*Oxford Centre for Collaborative Applied Mathematics, Mathematical Institute, University of Oxford, 24-29 St Giles', Oxford OX1 3LB, UK.*

⁴*Centre for Mathematical Biology, Mathematical Institute, University of Oxford, 24-29 St. Giles', Oxford OX1 3LB, UK. and*

⁵*Oxford Centre for Integrative Systems Biology, Department of Biochemistry, University of Oxford, South Parks Road OX1 3QU, UK.*

We show that a model reaction-diffusion system with two species in a monostable regime and over a large region of parameter space, produces Turing patterns coexisting with a limit cycle which cannot be discerned from the linear analysis. As a consequence, Turing patterns oscillate in time, a phenomenon which is expected to occur only in a three morphogen system. When varying a single parameter, a series of bifurcations lead to period doubling, quasi-periodic and chaotic oscillations without modifying the underlying Turing pattern. A Ruelle-Takens-Newhouse route to chaos is identified. We also examined the Turing conditions for obtaining a diffusion driven instability and discovered that the patterns obtained are not necessarily stationary for certain values of the diffusion coefficients. All this results demonstrates the limitations of the linear analysis for reaction-diffusion systems.

PACS numbers: 87.18.Hf, 05.45.Pq, 82.40.Bj

Reaction-diffusion systems can produce spatially periodic stationary patterns, usually known as Turing patterns. In his seminal work [1], Turing suggests the possibility of obtaining periodic patterns, both in time and space, which only occur with three or more morphogens. More recently, it has been shown that Turing patterns oscillating in time can be generated in a two-species system when Turing and Hopf instabilities interact [2], by coupling stationary Turing structures with oscillating layers [3] or in some bistable systems [4] where neither Hopf or wave instabilities are required.

Recently diffusion induced chaos has become very interesting, due to its connection with chemical chaos [5] and to the existence of some biological phenomena displaying this behavior [6]. Spatiotemporal chaos in reaction-diffusion systems can arise in different ways, for instance from the interaction between Turing and Hopf bifurcations [7], by homoclinic explosions [8], by the interaction with propagating fronts [9] or behind transitions fronts simulated by moving boundaries [10].

In this letter we study a simple reaction-diffusion system with two species in a monostable regime, and with a fixed domain size, which produces time oscillations and chaos in a region where linear analysis predicts only Turing patterns, with no oscillations. As a single parameter varies, the oscillating patterns undergo successive bifurcations, producing period doubling, torus and chaos. Furthermore, when the value of the ratio of diffusion coefficients fulfils the conditions for a Turing instability, we found the unexpected results that in a large region of parameter space only Turing patterns oscillating in

time emerge from the homogeneous steady state. The importance of these results is that it not only shows the stringent limitations of linear analysis but also opens new perspectives on the application of reaction-diffusion systems to real biological and chemical systems.

The reaction-diffusion model equations that we study in this work is the so-called BVAM model [11]:

$$\begin{aligned}\frac{\partial u}{\partial t} &= D\nabla^2 u + \eta(u + av - Cuv - uv^2), \\ \frac{\partial v}{\partial t} &= \nabla^2 v + \eta(bv + Hu + Cuv + uv^2),\end{aligned}\tag{1}$$

which presents a richness of behavior making it suitable as a good “laboratory” to gain insight into the mechanisms of pattern formation [12]. We will keep parameters D , C and H free while the remaining parameter values will be $\eta = 1$, $a = -1$, $b = -\frac{3}{2}$. According to linear analysis, this choice assures that the equilibrium point $(0, 0)$, in the absence of diffusion, is a stable spiral for the values of H considered in this work, and also that the trace of the Jacobian is negative, as we shall see below.

The diffusionless equation has the following equilibrium points

$$\begin{aligned}(u_0, v_0) &= (0, 0), \\ (u_{\mp}, v_{\mp}) &= \left(\frac{-5C \mp \sqrt{5}\sqrt{\Delta}}{4H + 4}, \frac{-5C \mp \sqrt{5}\sqrt{\Delta}}{10} \right),\end{aligned}$$

where $\Delta = 5C^2 - 8H + 12$. We observe that if $\Delta > 0$ three equilibrium points are present but if $\Delta < 0$ then $(0, 0)$ is the only real equilibrium point, hereafter denoted

as O . The particular case $\Delta = 0$ defines a saddle-node bifurcation curve defined by the equation (see Fig. 1),

$$H^{SN} = \frac{1}{8} (5C^2 + 12). \quad (2)$$

Along this curve, two equilibrium points are present and to the left of H^{SN} the three equilibrium points are recovered. In the following we consider parameter values C and H inside the shaded region in Fig. 1. The Jacobian evaluated at O is:

$$\mathbb{J}^0 = \begin{pmatrix} 1 & -1 \\ H & -\frac{3}{2} \end{pmatrix}.$$

From this we obtain $\lambda_{\mp} = \frac{1}{4} (-1 \mp \sqrt{25 - 16H})$, from which it is concluded that O is stable provided that $H > 3/2$, the value $H = 3/2$ corresponds to the minimum of H^{SN} . Thus, the shaded region bounded by H^{SN} in Fig. 1, corresponds to a monostable regime.

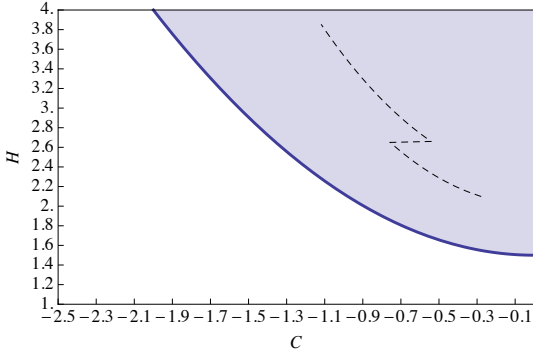


FIG. 1: The bold line is the saddle-node bifurcation curve (Eq. 2), of system (Eq. 1) without diffusion (only the region $C < 0$ is shown). In the shaded region, $(0,0)$ is the only equilibrium point, which is stable. The dashed curve is the locus of a Hopf bifurcation calculated numerically from (1), as described in the text.

The trace $\text{tr}(\mathbb{J}^0) = -1/2$ is always negative, consequently a Hopf bifurcation, which requires $\text{tr}(\mathbb{J}^0) = 0$, is not feasible. By considering diffusion in the linearized system, following the standard analysis for a Turing instability [13], we build up the matrix $\Gamma = \mathbb{J}^0 - k^2 \mathbb{D}$, where $\mathbb{D} = \text{diag}(D, 1)$, from which we find $\text{tr}(\Gamma) = -1/2 - (1 + D)k^2$. Since $D \geq 0$, it follows that $\text{tr}(\Gamma) < 0$, thus neither oscillations with $k \neq 0$ (wave bifurcation) are allowed and, consequently, linear analysis predicts no oscillations at all. Since O is linearly stable, there remains the possibility of having a Turing (diffusion-driven) instability. Using D as the bifurcation parameter, the conditions for a Turing instability [13] yield the critical values

$$k_c^2 = H - \frac{3}{2} + \sqrt{H \left(H - \frac{3}{2} \right)}, \quad (3)$$

$$D_c = \frac{8}{9} \left(H - \frac{3}{4} - \sqrt{H \left(H - \frac{3}{2} \right)} \right). \quad (4)$$

Notice that both critical quantities are independent of C .

The model in Eq. 1 was solved numerically in one dimension, with zero flux boundary conditions and random initial conditions around the equilibrium point $(0,0)$. The second partial derivative terms in (1) are discretized using finite differences, including zero flux boundary conditions in the discretization. Using a mesh with N nodes yields a set of $2N$ ordinary differential equations which were solved using the software library *CVODE* [14], with a numerically calculated Jacobian matrix. Scalar absolute and relative tolerances of 10^{-9} were used and $\Delta t = 0.01$. We set $N = 50$ and $\Delta x = 0.2$, thus the system size is $L = 9.8$.

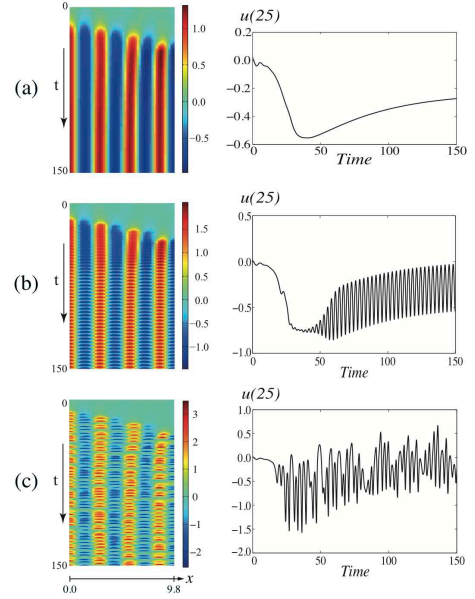


FIG. 2: Numerical simulations of the system (1) in 1D, for $H = 3$ and $D = 0.08$. The left column shows the space-time plot of u for three values of C (the plots for v are rather similar). On the right column, the time series registered at the central point, $u(25)$, of the corresponding space time patterns are shown. (a) $C = -0.6$, (b) $C = -1$ and (c) $C = -1.5$.

Since the critical parameters depend only on H , we first obtain a D_c valid for the range $\frac{3}{2} < H < 3.8$. In this interval D_c decreases monotonically, thus, we need to consider only the values of D_c when H is evaluated at the inequalities boundaries. From Eq. 4 we see that for $H = 3/2$, $D_c = 2/3 \approx 0.66$, and that for $H = 3.8$, $D_c \approx 0.083$. Thus if we set $D = 0.08$, Turing patterns should be produced in the range $\frac{3}{2} < H < 3.8$. We now consider C as a control parameter to explore its effect on the generated patterns. In what follows and unless otherwise indicated, we set $D = 0.08$ and $H = 3$. For this value of H , Eq. 3 gives $k_c \approx 1.9029$ and, from the dispersion relation, it is found that the most rapidly growing mode is $k \approx 2.1146$. Therefore, we expect a wavelength of $2\pi/2.1146 \approx .297$, or $9.8/2.97 \approx 3.3$ stripes in the simulations.

In Fig. 2 numerical simulations for three different values of C are displayed; in the left column, the space time plots for u , up to 15000 time iterations only ($t = 150$) are shown, for clarity. In the right column, the corresponding time series of the central point $u(25)$ are shown. As expected, for $C = -0.6$, as in Fig. 2(a) a stationary Turing pattern is obtained. When $C = -1$ (Fig. 2(b)), a stationary pattern is generated initially but eventually regular oscillations emerge. If C is decreased further, approaching the line H^{SN} , the pattern oscillates in an apparently chaotic fashion, as shown in Fig. 2(c) for $C = -1.5$. Since oscillations are not predicted by the linear analysis, and the conditions for a Turing instability are valid for these parameter values, it seems plausible to assume that they are a consequence of the non-linear terms and, in particular, of the relative strength of the quadratic and cubic nonlinearities, given by the magnitude of C . Since an analytical treatment of non-linearities is often prohibitive, we used the bifurcation software AUTO [15] to detect possible oscillatory instabilities.

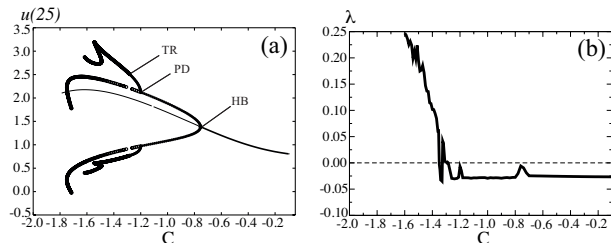


FIG. 3: (a) Numerically calculated bifurcation diagram of system (1) using AUTO; Supercritical Hopf (HB), period doubling (PD) and torus (TR) bifurcations are detected at $C = -0.7546515$, -1.200656 and -1.281831 , respectively. (b) Numerically calculated maximal Liapunov exponents.

In Fig. 3(a) we show the bifurcation diagram. As C decreases from -0.1 , the stable stationary (Turing) state loses stability through a supercritical Hopf bifurcation at $C = -0.7546515$ (successive bifurcations will be discussed afterwards). Bifurcation diagrams can be generated for different values of H so that a curve of Hopf bifurcations in a C vs. H plane can be calculated numerically. By using steps of 0.01 in H , the resulting curve are plotted in Fig. 1 as a dashed line. This curve separates the mono-stability region, where conditions for a Turing instability are satisfied, in two regions: in the right hand side of the Hopf curve Turing patterns are realised, and in the left patterns oscillate in time.

It is worth mentioning that in the interval $2.1 < H < 2.5$ no Hopf bifurcation occurs and in this region only oscillatory Turing patterns emerge from the homogeneous steady state, instead of the expected stationary patterns. We observe from Eq. 4 that D_c increases as H diminishes, such that when, for instance, $H = 1.8$ the critical value $D_c = 0.2801 \gg 0.08$. According to linear analysis, many modes become unstable and one expects that

the most rapidly growing mode will eventually dominate. However, numerical simulations show that this is not so: If D is just below 0.2801 Turing stationary pattern are obtained, as expected, but when $D \ll 0.2801$, only Turing patterns oscillating in time emerge from the homogeneous steady state.

Once the Hopf bifurcation line is crossed, if C decreases further, the oscillations become irregular, and near the H^{SN} line they appear to become chaotic. In Fig. 3(b), maximal Lyapunov exponents (λ) are plotted versus C . According to our numerical results, λ becomes zero at $C = -1.285$ and positive after this value, except for a small region of stability ($-1.33 \leq C \leq -1.35$). Consequently, chaos is expected when $-1.285 < C < -1.33$ and when $C < -1.35$.

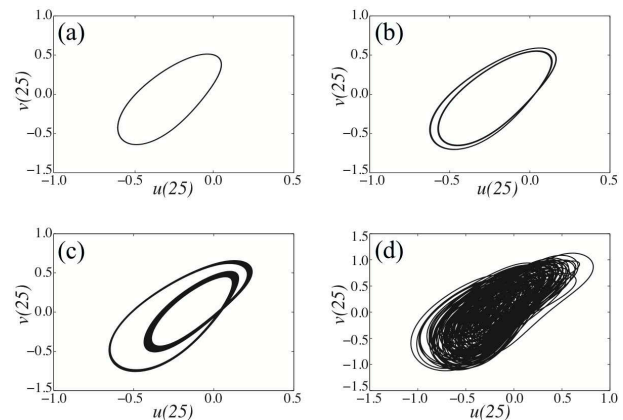


FIG. 4: Phase portraits of the central points for different values of C , after 50000 time iterations ($t = 500$). (a) $C = -1.15$, (b) $C = -1.21$, (c) $C = -1.285$ and (d) $C = -1.5$.

In Fig. 4, phase portraits are displayed for different values of C . After crossing the Hopf bifurcation line a limit cycle is formed, as shown in Fig. 4(a), for $C = -1.15$. If $C = -1.21$ the cycle doubles its period, as shown in Fig. 4(b). At smaller values of C a torus is generated at $C = -1.285$, as in Fig. 4(c), and chaotic orbits, shown in Fig. 4(d) appear for $C < -1.5$. All these results are consistent with the successive bifurcations displayed in the bifurcation diagram of Fig. 3(a): after the Hopf bifurcation (at $C = -0.7546515$), the limit cycle loses stability through a period-doubling for $C = -1.200656$ and this cycle itself loses stability through a torus at $C = -1.281831$.

The quasiperiodicity of the torus in Fig. 4(c) can be verified by calculating its power spectrum. In Fig. 5(a), the power spectrum for the torus ($C = -1.285$) is shown. The limit cycle after the Hopf bifurcation has frequency $\omega_1 = 0.338$, the period doubling introduces the frequency $\omega_1/2$ and the torus bifurcation introduces the new frequency, $\omega_2 = 0.282$, such that $\omega_1/\omega_2 = 1.19858156$ is a number that, up to numerical resolution is irrational. The power spectrum for $C = -1.455$, shown in the in-

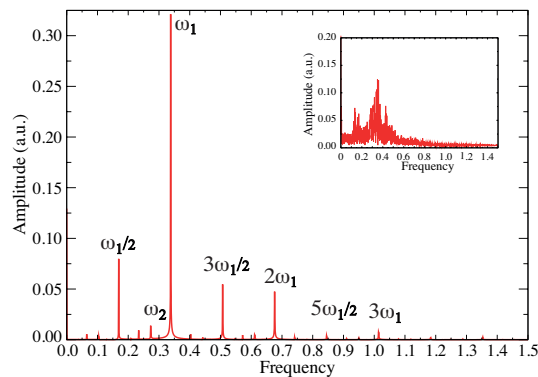


FIG. 5: Power spectrum for $C = -1.285$; the frequency $\omega_1 = 0.338$ and its integer multiples appear after the Hopf bifurcation; the period doubling introduces the frequency $\omega_1/2$ and the torus bifurcation $\omega_2 = 0.282$, where ω_1/ω_2 is, up to numerical resolution, an irrational number. Inset: Power spectrum for $C = -1.455$ showing a continuous band of frequencies, typical of a chaotic oscillation.

set of Fig. 5, exhibits a continuous band of frequencies, confirming the chaotic nature of the oscillation.

From all of these numerical results, we observe the following sequence of bifurcations: stationary \rightarrow Hopf \rightarrow 2-torus. Numerically, when a third frequency is about to appear (3-torus), small perturbations transform the quasiperiodic orbit into a chaotic orbit, or a strange attractor. This result is consistent with the well-known Ruelle-Takens-Newhouse route to chaos [16]. In two dimensions, the parameter C controls the type of Turing pattern, spots or stripes [11] so, by varying this parameter we can generate breathing spots or stripes, in a regular, quasiperiodic or chaotic fashion. Some illustrative movies of the numerical calculations are included as Supplementary Material.

In summary, we have studied a simple reaction-diffusion system that exhibits oscillations and chaos in a novel way. Turing patterns lose stability through a Hopf bifurcation which can not be discerned from present linear analysis techniques. The bifurcation parameter C is absent in the linear analysis and, as it varies, quasiperiodic and chaotic oscillations are generated in a large region of parameter space. A Ruelle-Takens-Newhouse route to chaos is identified. The main conclusion of this work is that linear analysis may be a stringent limitation for studying reaction-diffusion systems and that the

non-linearities play an important role, not only on stabilising a pattern, but also in producing unsuspected bifurcations.

This work was supported by CONACyT and DGAPA-UNAM, México, under grants 79641 and IN100310-3 respectively, and was based on work supported in part by Award No KUK-C1-013-04, made by King Abdullah University of Science and Technology (KAUST).

-
- [1] A.M. Turing, Philos. Trans. R. Soc. London B **237**, 37 (1952).
 - [2] L. Yang, M. Dolnik, A.M. Zhabotinsky and I.R. Epstein, Phys. Rev. Lett. **88**, 208303 (2002).
 - [3] L. Yang and I.R. Epstein, Phys. Rev. Lett. **90**, 178303 (2003).
 - [4] V.K. Vanag and I.R. Epstein, Phys. Rev. E **71**, 066212 (2005).
 - [5] Y. Kuramoto, *Chemical Oscillations, Waves and Turbulence* (Springer, Tokyo, 1984).
 - [6] L.F. Olsen and H. Degn, Q. Rev. Biophys. **18**, 165 (1985).
 - [7] A. De Wit, G. Dewel and P. Borckmans, Phys. Rev. E **48** R4191 (1993); V. Petrov, S. Metens, P. Borckmans and K. Showalter, Phys. Rev. Lett. **75** 2895 (1993).
 - [8] J. Elezgaray and A. Arneodo, Phys. Rev. Lett. **68**, 714 (1992).
 - [9] J.H. Merkin, V. Petrov, S.K. Scott and K. Showalter, Phys. Rev. Lett. **76**, 546 (1996).
 - [10] J.A. Sherratt, Dynam. Stab. Systems **11**, 303 (1996).
 - [11] R.A. Barrio, C. Varea, J.L. Aragón and P.K. Maini, *Bull. Math. Biol.*, **61**, 483 (1999); T. Leppänen, Ph.D. thesis, Helsinki University of Technology, 2004.
 - [12] C. Varea, J.L. Aragón and R.A. Barrio, Phys. Rev. E **60**, 4588 (1999); D.A. Striegel, M.K. Hurdal, Plos. Comput. Biol. **5**, e1000524 (2009); R.A. Barrio, R.E. Baker, B. Vaughan, JR., K. Tribuzy, M.R. de Carvalho, R. Basanezi and P.K. Maini, Phys. Rev. E. **79**, 031908 (2009); T.E. Woolley, R.E. Baker, P.K. Maini, J.L. Aragón and R. A. Barrio, Phys. Rev. E **82**, 051929 (2010).
 - [13] J.D. Murray, *Mathematical Biology*, Vol II (Springer, Berlin, 2002).
 - [14] S. D. Cohen and A. C. Hindmarsh, Comput. Phys. **10**, 138 (1996).
 - [15] B. Ermentrout, *Simulating, Analyzing, and Animating Dynamical Systems. A Guide to XPPAUT for Researchers and Students* (Society for Industrial Mathematics, Philadelphia, 2002).
 - [16] S. Newhouse, D. Ruelle and F. Takens, Comm. Math. Phys. **64**, 35 (1978); J.P. Eckmann, Rev. Mod. Phys. **53**, 643 (1981).

RECENT REPORTS

| | | |
|-------|----------------------------------------------------------------------------------------------------------------------------------------------------------------------|-------------------------------------------------------------------|
| 05/12 | Solute transport within porous biofilms: diffusion or dispersion? | Davit Byrne Osborne Pitt-Francis Gavaghan Quintard |
| 65/11 | Adaptive Finite Element Method Assisted by Stochastic Simulation of Chemical Systems | Cotter Vejchodsky Erban |
| 06/12 | Effects of intrinsic stochasticity on delayed reaction-diffusion patterning systems | Woolley Baker Gaffney Maini Seirin-Lee |
| 07/12 | Axial Dispersion via Shear-enhanced Diffusion in Colloidal Suspensions | Griffiths Stone |
| 08/12 | Qualitative Analysis of an Integro-Differential Equation Model of Periodic Chemotherapy | Jaina Byrne |
| 09/12 | Modeling Stem/Progenitor Cell-Induced Neovascularization and Oxygenation | Jain Moldovan Byrne |
| 10/12 | Allee Effects May Slow the Spread of Parasites in a Coastal Marine Ecosystem | Krkošek Connors Lewis Poulin |
| 11/12 | Parasite spill-back from domestic hosts may induce an Allee effect in wildlife hosts | Krkošek Ashander Lewis |
| 12/12 | Modelling temperature-dependent larval development and subsequent demographic Allee effects in adult populations of the alpine butterfly <i>Parnassius smintheus</i> | Wheeler Bampfylde Lewis |
| 13/12 | Putting “space” back into spatial ecology | Fortin Peres-Neto Lewis |
| 14/12 | Wildlife disease elimination and density dependence | Potapova Merrill Lewis |
| 15/12 | Spreading Speed, Traveling Waves, and Minimal Domain Size in Impulsive Reaction-diffusion Models | Lewis Li |
| 16/12 | MCMC methods for functions modifying old algorithms to make them faster | Cotter Roberts Stuart White |
| 17/12 | Weyl Geometry and the Nonlinear Mechanics of Distributed Point Defects | Yavari Goriely |

| | | |
|-------|-----------------------------------------------------------------------------------------------------------------------------------------|------------------------------------------------------------------------------------------------------|
| 18/12 | A note on oblique water entry | Moore Howison Ockendon Oliver |
| 19/12 | Calculus on surfaces with general closest point functions | März Macdonald |
| 20/12 | Multiple equilibria in a simple elastocapillary system | Taroni Vella |
| 21/12 | Multiphase modelling of vascular tumour growth in two spatial dimensions | Hubbard Byrne |
| 22/12 | Chebfun and Numerical Quadrature | Hale Trefethen |
| 23/12 | Moment-based formulation of NavierMaxwell slip boundary conditions for lattice Boltzmann simulations of rarefied flows in microchannels | Reis Dellar |
| 24/12 | Correspondence between one- and two-equation models for solute transport in two-region heterogeneous porous media | Davit Wood Debenest Quintard |
| 25/12 | Rolie-Poly fluid flowing through constrictions: Two distinct instabilities | Reis Wilson |
| 26/12 | Age related changes in speed and mechanism of adult skeletal muscle stem cell migration | Collins-Hooper Woolley Dyson Patell Potter Baker Gaffney Maini Dash Patel |
| 27/12 | The interplay between tissue growth and scaffold degradation in engineered tissue constructs | ODea Osborne El Haj Byrne Waters |

Copies of these, and any other OCCAM reports can be obtained from:

Oxford Centre for Collaborative Applied Mathematics
Mathematical Institute
24 - 29 St Giles'
Oxford
OX1 3LB
England
www.maths.ox.ac.uk/occam